Experimental Mechanics (2024) 64:3–19
https://doi.org/10.1007/s11340-023-01005-1

REVIEW ARTICLE

On Orthotropic Elastic Constitutive Modeling for Springback Prediction

Y. Zhang[1,2] · Y. Duan[1,2] · P. Fu[1,2] · S. Qi[1,2] · J. Zhao[1,2]

Received: 10 July 2023 / Accepted: 28 September 2023 / Published online: 17 October 2023

Abstract

Background The conventional isotropic elastic model neglects the anisotropy of sheet metals' elastic modulus, leading to inevitable errors in springback prediction.

Objective Aiming at the problem of anisotropic springback in the forming process of sheet metals, an orthotropic elastic model was established in this study, and the applicability of the model was analyzed. An accurate and convenient numerical solution method was proposed, considering the challenge of calibrating model parameters through experimental measurement.

Methods The reliability of the proposed parameter solution method is verified by uniaxial tensile and thin-walled tube torsion tests. To verify the anisotropic elastic model, both V-bending finite element simulation and experimental testing were conducted.

Results The proposed parameter solution method has good prediction accuracy, with an average relative error within 5%. The three-group sample solution method significantly reduces experimental and data processing workload, demonstrating the precision and user-friendliness of this method. The proposed model yields a significant enhancement in springback prediction accuracy when compared to the conventional isotropic elastic model.

Conclusion This study is basic research on the prediction of anisotropic springback, which can improve the simulation accuracy of the sheet metals forming process involving this problem, particularly in the anisotropic metal sheet stamping process.

Keywords Anisotropy · Elastic constitutive · Parameter calibration · Springback · Simulation

Introduction

The springback phenomenon is a significant engineering problem that arises in the production of sheet metal-formed products. The occurrence of springback after unloading of the forming tool will result in additional deviations in the shape and size of the parts. This was more pronounced during sheet metal forming compared to other methods of forming (i.e. bulk forming) [1, 2], owing to the small thickness of the material.

Sheet metals usually exhibit a certain initial elastic anisotropy mainly due to crystallographic texture, which is caused by the previous production steps rolling and annealing [3]. During the process of sheet metals forming, every particle on the part undergoes elastic–plastic loading and unloading, in which plastic loading and unloading are also accompanied by elastic deformation. The elastic deformation exerts a significant influence on the accumulation of plastic deformation and the accuracy of springback prediction [4]. The accuracy of describing elastic deformation is closely related to the adopted elastic constitutive model. However, the conventional isotropic elastic model neglects the anisotropy of sheet metals' elastic modulus, leading to inevitable errors in springback prediction. The anisotropic elastic properties of the rolled sheet make it necessary to consider the impact of this difference in springback prediction, and compensation for springback in different directions must also be adjusted accordingly. In other words, for example, the elastic modulus of the sheet metal rolling

✉ Y. Duan
yongchuan.duan@ysu.edu.cn

Y. Zhang
zy802321@stumail.ysu.edu.cn

P. Fu
pengchengfu@stumail.ysu.edu.cn

S. Qi
ShaocongQi@stumail.ysu.edu.cn

J. Zhao
zhaojun@ysu.edu.cn

[1] Key Laboratory of Advanced Forging & Stamping Technology and Science (Yanshan University), Ministry of Education of China, Qinhuangdao City, People's Republic of China 066004

[2] College of Mechanical Engineering, Yanshan University, Qinhuangdao City, People's Republic of China 066004

direction and the vertical direction are not equal, then the amount of springback will also be different. Therefore, it is crucial to establish a constitutive model that can precisely describe the anisotropic elastic behavior for accurate prediction of part forming and springback.

Over the past few years, the research on elastic modulus mainly focuses on the nonlinear evolution of elastic modulus. The elastic modulus of certain materials exhibits significant deviation after plastic deformation, prompting numerous scholars to conduct research on such materials with varying elastic modulus. Yoshida and Amaishi [4] proposed an evolution model of elastic modulus to describe the nonlinear stress-strain response during the unloading–reloading process. Sun and Wagoner [5] observed that the unloading modulus was reduced by 30% compared to Young's modulus by loading and unloading DP780 and DP980 steels. Zajkani and Hajbarati [6, 7] captured the variable unloading modulus through the nonlinear function of plastic strain. Meng et al. [8] applied the nonlinear elastic model proposed by Yoshida and Amaishi to the springback prediction of 6061 aluminum alloy. Chang et al. [9] analyzed the variation of unloading elastic modulus and inelastic recovery with strain through cyclic loading-unloading tests and established a correlation model between unloading elastic modulus and real plastic strain. Aerens et al. [10] considered the evolution of elastic modulus to study the relationship between the angle accuracy of air bending and the calculated stroke accuracy. Liu et al. [11] proposed a mathematical model considering the evolution of elastic modulus and applied it to three-dimensional finite element analysis to simulate the cold rolling process. Yang et al. [12] developed an analytical model considering the change of elastic modulus to predict the springback of advanced high-strength steel in air bending. Mehrabi et al. [13] proposed a new analytical method to predict the bending and springback behavior of hexagonal close-packed metal sheets by combining the variable elastic modulus method. The above reports have studied the influence of elastic modulus degradation on springback during unloading and reloading, but neglected the directionality of elastic modulus, that is, anisotropic elasticity. It appears that scholars have not given sufficient attention to the anisotropic elasticity aspect of the springback problem.

In addition to the variable elastic modulus discussed above, the study of springback mainly focuses on the hardening model, complex loading and anisotropic yield function. The Yoshida-Uemori (Y-U) nonlinear hardening model [14–19] and Chaboche kinematic hardening model [20–22] were used to study the springback. Choi et al. [23] improved the Homogeneous anisotropic hardening model (HAH) to predict springback. Julsri et al. [24] explained the effect of material hardening on the springback prediction of advanced high strength steel based on microstructure modeling. Sumikawa et al. [25, 26] proposed a new material model considering nonlinear behavior and applied it to the pressing test and corresponding springback analysis of bent hat-shaped parts. Leu [27], Zhu et al. [28], Ouakdi et al. [29], Zhai et al. [30], Wang et al. [31], Kut et al. [32], Zhan et al. [33] studied the influence of complex loading on springback. In recent studies, the anisotropic yield criterion was introduced into the study of springback prediction [34–38]. However, Marko et al. [39] given the conclusion that accurate modelling only of anisotropic yielding was not enough to accurately predict the springback phenomenon. The constitutive model should also include the strain path-dependent change of the elastic modulus. When most studies above do not center on the elastic modulus, in order to simplify, the elastic model is treated as isotropic linear elasticity, which undoubtedly increases the error of springback prediction.

The accuracy of the anisotropic elastic model's description is directly dependent on the quality of experimental data used to calibrate its coefficients, which include elastic modulus, Poisson's ratio and shear modulus. The elastic modulus and Poisson's ratio can be determined through uniaxial tensile tests conducted at various angles relative to the rolling direction of the sheet. However, due to the negligible elastic deformation in the thickness direction of metal sheets, it is impractical to experimentally measure or calculate the elastic parameters in this direction using volume invariance as applied to plastic deformation. The shear modulus can be obtained by pure shear test. Although effective shear stress-strain curves can be obtained by tensile shear tests, but there is always a risk of instability failure [40, 41].Therefore, the torsional shear test is selected avoid this situation. Ballo et al. [42] and Bhaduri [43] theoretically analyzed and experimentally verified the feasibility of thin-walled tube torsion experiments. However, implementing torsion experiments on metal sheets poses numerous challenges. Firstly, the sheet must be rolled into a slender tube and welded, which is a complex process. Secondly, thin-walled tube torsion experiments may result in failure problems such as torsional instability or damage at both ends due to loading forces. Thus, many special tube torsion specimens were designed [44–47]. From the preceding discussion, it is evident that both the elastic parameters pertaining to thickness direction and shear modulus are difficult to measure experimentally. Therefore, a convenient approach is required for obtaining these parameters.

The current research on springback is primarily focused on the field of sheet metals stamping, and further investigation into the influence of anisotropic elastic properties unique to rolled sheet metals on this issue is necessary. The paper is organized as follows. The orthotropic two-dimensional elastic constitutive model for metal sheets is established in "Elasticity constitutive model" section and then a necessary and sufficient condition to assess its applicability is proposed in "Analysis of model applicability" section. Based on this, a

practical numerical solution method called the error function extremum method (ERFM) was proposed for calibrating model parameters in "Calibration method of elastic parameters" section. In "Experiment" section, experiments to obtain input data and validation data were carried out. We finally discuss in "Results and discussions" section the reliability of the parameters solving method and the superiority of the orthotropic elastic model.

Elasticity Constitutive Model

Isotropic Elastic Model

If a material exhibits identical mechanical properties in all directions, it is considered isotropic. In such cases, only two independent coefficients are required for the elastic constitutive relation. The isotropic elastic constitutive relation is expressed as

$$\begin{bmatrix} \sigma_x \\ \sigma_y \\ \sigma_z \\ \tau_{yz} \\ \tau_{zx} \\ \tau_{xy} \end{bmatrix} = \frac{E}{(1+\nu)(1-2\nu)} \begin{bmatrix} 1-\nu & \nu & \nu & 0 & 0 & 0 \\ \nu & 1-\nu & \nu & 0 & 0 & 0 \\ \nu & \nu & 1-\nu & 0 & 0 & 0 \\ 0 & 0 & 0 & \frac{1-2\nu}{2} & 0 & 0 \\ 0 & 0 & 0 & 0 & \frac{1-2\nu}{2} & 0 \\ 0 & 0 & 0 & 0 & 0 & \frac{1-2\nu}{2} \end{bmatrix} \begin{bmatrix} \varepsilon_x \\ \varepsilon_y \\ \varepsilon_z \\ \gamma_{yz} \\ \gamma_{zx} \\ \gamma_{xy} \end{bmatrix} \tag{1}$$

where E and ν are elastic constants.

The shear modulus can be expressed as

$$G = \frac{E}{2(1+\nu)} \tag{2}$$

Orthotropic Elastic Model

The orthotropic elastic constitutive model is based on three basic assumptions: The metal sheet possesses three anisotropic principal axes that are mutually perpendicular to each other; The metal sheet exhibits linear elasticity in elastic deformation; The metal sheet is subjected to a two-dimensional plane stress state.

Concepts and definitions

The three spindles are identified by the numbers 1, 2 and 3. Without loss of generality, assume that the 1-axis is aligned with the rolling direction of the metal sheet. A uniaxial tensile specimen can be used to determine the elastic modulus and two Poisson's ratios. By conducting a uniaxial tensile test along the 1-axis, three experimental values of E_1, ν_{12} and ν_{13} can be obtained as an example. The setting of the material spindle and reference coordinate system is shown in Fig. 1.

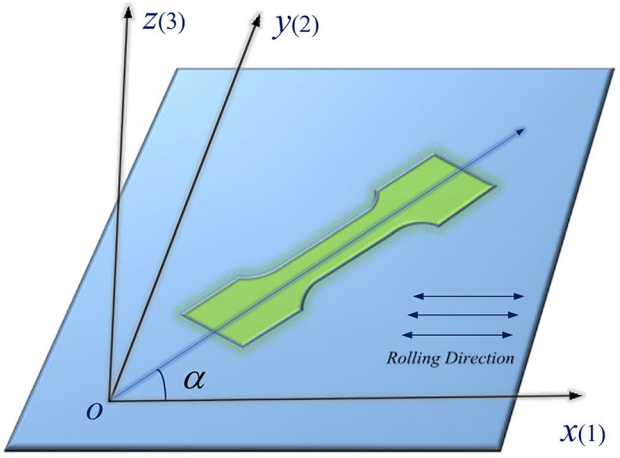

Fig. 1 Material spindle and reference axis setting, where α is the sampling angle of the uniaxial tensile specimen relative to the rolling direction

Constitutive equation

For general anisotropic linear elastic materials, stress and strain have a linear relationship. It is

$$\{\varepsilon_i\} = [S_{ij}]\{\sigma_j\} \tag{3}$$

where $\{\varepsilon_i\} = \{\varepsilon_x, \varepsilon_y, \varepsilon_z, \gamma_{yz}, \gamma_{zx}, \gamma_{xy}\}^{\mathrm{T}}$ is strain vector, $\{\sigma_i\} = \{\sigma_x, \sigma_y, \sigma_z, \tau_{yz}, \tau_{zx}, \tau_{xy}\}^{\mathrm{T}}$ is stress vector, $[S_{ij}]$ is flexibility matrix, $i, j = 1,2,3\ldots6$. From the energy density of elastic deformation, it can be proved that the flexibility matrix is a symmetric matrix. Therefore, only twenty-one of the thirty-six coefficients in the matrix are independent.

From the energy density of elastic deformation and symmetry, it can be proved that only nine coefficients in the flexibility matrix are independent, while all remaining coefficients are equal to zero. Under a two-dimensional plane stress state, there are $\sigma_z = \tau_{yz} = \tau_{zx} = 0, \gamma_{yz} = \gamma_{zx} = 0$. The expression of the constitutive equation matrix for an orthotropic metal sheet subjected to a two-dimensional plane stress state is therefore as follows:

$$\begin{Bmatrix} \varepsilon_x \\ \varepsilon_y \\ \varepsilon_z \\ 0 \\ 0 \\ \gamma_{xy} \end{Bmatrix} = \begin{bmatrix} S_{11} & S_{12} & S_{13} & 0 & 0 & 0 \\ & S_{22} & S_{23} & 0 & 0 & 0 \\ & & S_{33} & 0 & 0 & 0 \\ & & & S_{44} & 0 & 0 \\ & symmetry & & & S_{55} & 0 \\ & & & & & 0 \end{bmatrix} \begin{Bmatrix} \sigma_x \\ \sigma_y \\ 0 \\ 0 \\ 0 \\ \tau_{xy} \end{Bmatrix} \tag{4}$$

Obviously, when equation (4) is expanded, the coefficients S_{33}, S_{44} and S_{55} are absent in the constitutive equation. There are only six independent undetermined coefficients in equation (5) now.

$$\begin{cases} \varepsilon_x = S_{11}\sigma_x + S_{12}\sigma_y \\ \varepsilon_y = S_{21}\sigma_x + S_{22}\sigma_y \\ \varepsilon_z = S_{31}\sigma_x + S_{32}\sigma_y \\ \gamma_{xy} = S_{66}\tau_{xy} \end{cases} \quad S_{12} = S_{21} \tag{5}$$

The uniaxial tensile test conducted in the 1-axis direction obtains E_1, ν_{12}, and ν_{13}; while that performed in the 2-axis direction provides E_2, ν_{21}, and ν_{23}. Additionally, a pure shear test on the section aligned with the x-axis can determine G_{12}. By substituting these experimental values into equation (5), the anisotropic undetermined coefficients can be obtained. There are

$$\begin{cases} S_{11} = \dfrac{1}{E_1} \quad , \quad S_{12} = \dfrac{-\nu_{21}}{E_2} \\ S_{21} = \dfrac{-\nu_{12}}{E_1} \quad , \quad S_{22} = \dfrac{1}{E_2} \\ S_{13} = \dfrac{-\nu_{13}}{E_1} \quad , \quad S_{23} = \dfrac{-\nu_{23}}{E_2} \\ S_{66} = \dfrac{1}{G_{12}} \end{cases} \tag{6}$$

Analysis of Model Applicability

To assess the applicability of the orthotropic elastic model, necessary and sufficient conditions for evaluating linearly elastic orthotropic metal sheets were established based on fundamental definitions of elastic modulus and Poisson's ratio. In this study, the metal sheet that satisfies the orthotropic elastic constitutive equation and its corresponding stress-strain relationship is referred to as an orthotropic metal sheet; otherwise, it is classified as a non-orthogonal anisotropic metal sheet.

Necessary Condition

According to equation (5), there is $S_{12} = S_{21}$. It is

$$\frac{\nu_{12}}{E_1} = \frac{\nu_{21}}{E_2} \tag{7}$$

Equation (7) indicates that the elastic coefficient of the orthotropic metal sheet must meet the aforementioned relationship, which is a necessary condition for judging the orthotropic metal sheet.

Sufficient Condition

Due to the orthogonal anisotropy of the metal sheet, both elastic modulus and Poisson's ratio can be considered as functions of the sampling azimuth angleα (as shown in Fig. 1). When subjected to uniaxial tension along any direction, tensor transformation relationship can be obtained as

$$\sigma_x = \sigma_\alpha \cos^2\alpha \ , \ \sigma_y = \sigma_\alpha \sin^2\alpha \ , \ \tau_{xy} = \sigma_\alpha \sin\alpha\cos\alpha \tag{8}$$

$$\varepsilon_\alpha = \varepsilon_x \cos^2\alpha + \varepsilon_y \sin^2\alpha + \gamma_{xy}\sin\alpha\cos\alpha \tag{9}$$

$$\varepsilon_{\alpha+\frac{\pi}{2}} = \varepsilon_x \sin^2\alpha + \varepsilon_y \cos^2\alpha - \gamma_{xy}\ \sin\ \alpha\ \cos\ \alpha \tag{10}$$

Substituting equation (8) into equation (5), and then into equations (9) and (10), there are

$$\varepsilon_\alpha = S_{11}\sigma_\alpha \cos^4\alpha + S_{22}\sigma_\alpha \sin^4\alpha + \sigma_\alpha\left(2S_{12} + S_{66}\right)\sin^2\alpha\cos^2\alpha \tag{11}$$

$$\varepsilon_{\alpha+\frac{\pi}{2}} = \sigma_\alpha\left(S_{11} + S_{22} - 2S_{12} - S_{66}\right)\sin^2\alpha\cos^2\alpha + \sigma_\alpha S_{12} \tag{12}$$

$$\varepsilon_z = -\sigma_\alpha\left(S_{31}\cos^2\alpha + S_{32}\sin^2\alpha\right) \tag{13}$$

According to the aforementioned definitions of elastic modulus, width Poisson's ratio and thickness Poisson's ratio, there are

$$E(\alpha) = \frac{\sigma_\alpha}{\varepsilon_\alpha} = \frac{1}{S_{11}\cos^4\alpha + S_{22}\sin^4\alpha + \left(2S_{12} + S_{66}\right)\sin^2\alpha\cos^2\alpha} \tag{14}$$

$$\nu(\alpha) = -\frac{\varepsilon_{\alpha+\frac{\pi}{2}}}{\varepsilon_\alpha} = \frac{\left(S_{66} - S_{11} - S_{22} + 2S_{12}\right)\sin^2\alpha\cos^2\alpha - S_{12}}{S_{11}\cos^4\alpha + S_{22}\sin^4\alpha + \left(2S_{12} + S_{66}\right)\sin^2\alpha\cos^2\alpha} \tag{15}$$

$$\nu_t(\alpha) = -\frac{\varepsilon_z}{\varepsilon_\alpha} = \frac{-\left(S_{31}\cos^2\alpha + S_{32}\sin^2\alpha\right)}{S_{11}\cos^4\alpha + S_{22}\sin^4\alpha + \left(2S_{12} + S_{66}\right)\sin^2\alpha\cos^2\alpha} \tag{16}$$

where the domain of α is $[0, \frac{\pi}{2}]$. Therefore, when uniaxial tension is sampled in arbitrary direction α, the corresponding elastic modulus, width Poisson's ratio and thickness Poisson's ratio are substituted into equatios (14), (15) and (16). Three equations can be obtained, in which only S_{66} remains unknown while the remaining parameters are

determined by equation (6). Therefore, there must exist two equations that are independent.

Make

$$x = S_{11}\cos^4\alpha + S_{22}\sin^4\alpha + (2S_{12} + S_{66})\sin^2\alpha\cos^2\alpha \quad (17)$$

There is

$$(2S_{12} + S_{66})\sin^2\alpha\cos^2\alpha = x - (S_{11}\cos^4\alpha + S_{22}\sin^4\alpha) \quad (18)$$

Substituting equation (18) into equations (14) and (15), there is

$$\begin{cases} x \cdot E(\alpha) = 1 \\ x \cdot v(\alpha) = x - \left(S_{11}\cos^4\alpha + S_{22}\sin^4\alpha\right) - \left(S_{11} + S_{22}\right)\sin^2\alpha\cos^2\alpha - 2S_{12} \end{cases} \quad (19)$$

That is

$$\frac{1 - v(\alpha)}{E(\alpha)} = S_{11}\cos^2\alpha + S_{22}\sin^2\alpha + 2S_{12} \quad (20)$$

Similarly, solving equations (14) and (16) simultaneously can obtain

$$\frac{v_t(\alpha)}{E(\alpha)} = -S_{31}\cos^2\alpha - S_{32}\sin^2\alpha \quad (21)$$

Substituting equations (6) and (7) into equations (20) and (21), the sufficient condition for judging the orthotropic metal sheet is established.

$$\begin{cases} \frac{1-v(\alpha)}{E(\alpha)} = \frac{1}{E_1}\cos^2\alpha + \frac{1}{E_2}\sin^2\alpha - \frac{1}{2}\left(\frac{v_{12}}{E_1} + \frac{v_{21}}{E_2}\right) \\ \frac{v_t(\alpha)}{E(\alpha)} = \frac{v_{13}}{E_1}\cos^2\alpha + \frac{v_{23}}{E_2}\sin^2\alpha \end{cases} \quad (22)$$

Equation (22) indicates that, in the case of orthotropic metal sheets, the uniaxial tensile test values along arbitrary directions must satisfy the above relationship. Thus, the necessary and sufficient conditions for distinguishing orthotropic metal sheets have been established. The necessary and sufficient conditions show that the true orthotropic metal sheet is only the one that satisfies both necessary and sufficient conditions. When the necessary and sufficient conditions are satisfied, equation (5) can yield more precise prediction results.

Obviously, when $E_1 = E_2, \nu_{12} = \nu_{21} = \nu_{13} = \nu_{23}$, the isotropic elastic constitutive also conforms to the above necessary and sufficient conditions. It can be seen that isotropic elastic constitutive is only an ideal case of orthotropic elastic constitutive. Therefore, the orthotropic elastic constitutive can more comprehensively and truly characterize the elastic deformation behavior of materials.

Calibration Method of Elastic Parameters

The parameters of the orthotropic elastic model involve Poisson's ratio in the thickness direction and shear modulus, which are difficult to measure by experiment. Additionally, most metal sheets generally do not strictly meet the above necessary and sufficient conditions. Therefore, a numerical method for solving elastic parameters is established based on the approximate satisfaction degree of different types of metal sheets to necessary and sufficient conditions, that is, the error extreme value function method.

The Orthotropic Metal Sheet

For the orthotropic metal sheet, all the anisotropic parameters except S_{66} in equation (5) can be determined through uniaxial tensile tests conducted along the material's principal 1-axes and 2-axes directions. Then S_{66} can be uniquely determined by any one of the equations (14–16). α is an arbitrary value between $[0, \frac{\pi}{2}]$. Without losing generality, take $[\alpha = \frac{\pi}{4}$, and substitute equation (6) into equation (14). After simplification, it can be obtained as

$$\frac{1}{G_{12}} = S_{66} = \frac{4}{E\left(\frac{\pi}{4}\right)} - \left(\frac{1 - v_{12}}{E_1} + \frac{1 - v_{21}}{E_2}\right) \quad (23)$$

Substituting $\alpha = \frac{\pi}{4}$ into equation (22), there is

$$\begin{cases} \frac{1-v\left(\frac{\pi}{4}\right)}{E\left(\frac{\pi}{4}\right)} = \frac{1}{2}\left(\frac{1-v_{12}}{E_1} + \frac{1-v_{21}}{E_2}\right) \\ \frac{v\left(\frac{\pi}{4}\right)}{E\left(\frac{\pi}{4}\right)} = \frac{1}{2}\left(\frac{v_{13}}{E_1} + \frac{v_{23}}{E_2}\right) \end{cases} \quad (24)$$

Substituting the first equation in equation (24) into equation (23) is

$$S_{66} = \frac{2\left(1 + v\left(\frac{\pi}{4}\right)\right)}{E\left(\frac{\pi}{4}\right)} \quad (25)$$

That is

$$G_{12} = \frac{E\left(\frac{\pi}{4}\right)}{2(1 + v\left(\frac{\pi}{4}\right))} \quad (26)$$

It can be seen from equation (26) that the shear modulus of the orthotropic metal sheet can be indirectly obtained through uniaxial tensile testing in direction $\alpha = \frac{\pi}{4}$.

The Non-orthogonal Anisotropic Metal Sheet

For non-orthogonal anisotropic metal sheets, the comprehensive error function methods for solving the approximate values of anisotropic elastic parameters are established. Make the experimental data obtained from uniaxial tension along the direction α_i be $E^{(i)}, \nu^{(i)}, \nu_t{}^{(i)}$ $(i = 1, 2, ...n)$, then the comprehensive relative error function can be constructed from the equations (14–16). Where $S = (S_{11}, S_{12}, S_{13}, S_{22}, S_{23}, S_{66})$.

$$\phi(S) = \sum_{i=1}^{n}\left[\left(\frac{E(\alpha_i)}{E^{(i)}} - 1\right)^2 + \left(\frac{\nu(\alpha_i)}{\nu^{(i)}} - 1\right)^2 + \left(\frac{\nu_t(\alpha_i)}{\nu_t{}^{(i)}} - 1\right)^2\right] \tag{27}$$

Unconstrained extremum value method for multi-group samples

Within the domain $\left[0, \frac{\pi}{2}\right]$ of α, n groups of experimental data $E^{(i)}, \nu^{(i)}, \nu_t{}^{(i)}$ $(i = 1, 2, ...n)$ can be obtained by n groups of uniaxial tension samples. Making the fitting function of experimental data are

$$\bar{E}(\alpha) = f(\alpha)\,, \quad \bar{\nu} = g(\alpha)\,, \quad \bar{\nu}_t = h(\alpha) \tag{28}$$

Then the error function equation (27) can be written in integral form. It is

$$\phi(S) = \int_0^{\frac{\pi}{2}}\left[\left(\frac{E(\alpha)}{f(\alpha)} - 1\right)^2 + \left(\frac{\nu(\alpha)}{g(\alpha)} - 1\right)^2 + \left(\frac{\nu_t(\alpha)}{h(\alpha)} - 1\right)^2\right]\mathrm{d}\alpha \tag{29}$$

When the metal sheet does not meet either the necessary condition or the sufficient condition, the anisotropy coefficient S can be obtained by solving the extremum stagnation point of the multivariate function equation (29).

Endpoint constraint condition extremum method for multi-group samples

When the metal sheet satisfies only the necessary conditions, the endpoint constraint conditions are introduced. That is

$$\begin{cases} E(0) = E_1, \nu(0) = \nu_{12}, \nu_t(0) = \nu_{13} \\ E\left(\frac{\pi}{2}\right) = E_2, \nu\left(\frac{\pi}{2}\right) = \nu_{21}, \nu_t\left(\frac{\pi}{2}\right) = \nu_{23} \end{cases} \tag{30}$$

Substituting equation (30) into equations (14–16) are

$$\begin{cases} S_{11} = \frac{1}{E_1}, S_{12} = -\frac{\nu_{21}}{E_2} \\ S_{21} = -\frac{\nu_{12}}{E_1}, S_{22} = \frac{1}{E_2} \\ S_{13} = -\frac{\nu_{13}}{E_1}, S_{23} = -\frac{\nu_{23}}{E_2} \end{cases} \tag{31}$$

Under the constraint condition of equation (31), S_{66} can be obtained by solving the conditional extremum stagnation point of equation (29). It is worth noting that, in this case, the fitting function equation (28) of the experimental data should also satisfy the endpoint constraints. There are

$$\begin{cases} f(0) = E_1, g(0) = \nu_{12}, h(0) = \nu_{13} \\ f\left(\frac{\pi}{2}\right) = E_2, g\left(\frac{\pi}{2}\right) = \nu_{21}, h\left(\frac{\pi}{2}\right) = \nu_{23} \end{cases} \tag{32}$$

Unconstrained extremum method for three-group samples

In order to minimize the amount of experiments and data processing, it is necessary to analyze and compare the accuracy of the elastic anisotropy coefficients obtained from the uniaxial tensile test data in the directions $\alpha = 0, \frac{\pi}{4}, \frac{\pi}{2}$.When three-group experiment data are used, $i = 1, 2, 3$ in equation (29) corresponds to $\alpha_i = 0, \frac{\pi}{4}, \frac{\pi}{2}$, and the error function is the sum of nine items. It can be seen from the equations (14–16) that

$$\begin{cases} E(0) = \frac{1}{S_{11}}, \nu(0) = -\frac{S_{12}}{S_{11}}, \nu_t(0) = -\frac{S_{13}}{S_{11}} \\ E\left(\frac{\pi}{4}\right) = \frac{4}{(S_{66} + 2S_{12}) + S_{11} + S_{22}} \\ \nu\left(\frac{\pi}{4}\right) = \frac{(S_{66} - 2S_{12}) - S_{11} - S_{22}}{(S_{66} + 2S_{12}) + S_{11} + S_{22}} \\ \nu_t\left(\frac{\pi}{4}\right) = \frac{-2(S_{13} + S_{23})}{(S_{66} + 2S_{12}) + S_{11} + S_{22}} \\ E\left(\frac{\pi}{2}\right) = \frac{1}{S_{22}}, \nu\left(\frac{\pi}{2}\right) = -\frac{S_{12}}{S_{22}}, \nu_t\left(\frac{\pi}{2}\right) = -\frac{S_{23}}{S_{22}} \end{cases} \tag{33}$$

When the metal sheet does not meet either the necessary or the sufficient conditions, the anisotropic coefficient S can be obtained by substituting equation (33) into equation (27) and solving the unconstrained extremum stationary point of the error function.

Endpoint constraint condition extremum method for three-group samples

When the metal sheet only meets the necessary conditions, the endpoint constraint condition equation (30) is introduced. Under the constraint condition equation (31), there are only three items in the error function equation (29). It is

$$\phi(S)=\left(\frac{E\left(\frac{\pi}{4}\right)}{E^{(2)}}-1\right)^2+\left(\frac{\nu\left(\frac{\pi}{4}\right)}{\nu^{(2)}}-1\right)^2+\left(\frac{\nu_t\left(\frac{\pi}{4}\right)}{\nu_t^{(2)}}-1\right)^2 \tag{34}$$

where $E^{(2)}$ is the elastic modulus of the uniaxial tensile sample in direction $\alpha=\frac{\pi}{4}$, $\nu^{(2)}$ is the corresponding Poisson's ratio in the width direction, $\nu_t{}^{(2)}$ is the corresponding Poisson's ratio in the thickness direction. For the convenience of the following derivation, it is expressed by E_{45}, ν_{45} and ν_{t45}, respectively. Substituting equation (33) into equation (34) is

$$\begin{aligned}\phi(S)=&\left(\frac{4}{E_{45}}\frac{1}{S_{66}+S_{11}+S_{22}+S_{12}+S_{21}}-1\right)^2\\&+\left(\frac{1}{\nu_{45}}\frac{S_{66}-S_{11}-S_{22}-S_{12}-S_{21}}{S_{66}+S_{11}+S_{22}+S_{12}+S_{21}}-1\right)^2\\&+\left(\frac{1}{\nu_{t45}}\frac{2\left(S_{13}+S_{23}\right)}{S_{66}+S_{11}+S_{22}+S_{12}+S_{21}}+1\right)^2\end{aligned} \tag{35}$$

It can be seen from the constraint equation (32) that only S_{66} remains to be determined in equation (34). So, make

$$\begin{cases}x=S_{66}+S_{11}+S_{22}+S_{12}+S_{21}\\a=\frac{4}{E_{45}},b=\frac{1}{\nu_{45}},c=2\left(S_{11}+S_{22}+S_{12}+S_{21}\right)\\d=\frac{2}{\nu_{t45}}\left(S_{13}+S_{23}\right)\end{cases} \tag{36}$$

Then equation (35) is simplified to

$$\phi(x)=\left(\frac{a}{x}-1\right)^2+\left(b\cdot\frac{x-c}{x}-1\right)^2+\left(\frac{d}{x}-1\right)^2 \tag{37}$$

Make $\frac{d_\phi}{dS_{66}}=\frac{d_\phi}{dx}\cdot\frac{dx}{dS_{66}}=0$, there is $\frac{d_\varnothing}{dx}=0$. That is

$$-\frac{a}{x^2}\left(\frac{a}{x}-1\right)+\frac{bc}{x^2}\left(b\cdot\frac{x-c}{x}-1\right)-\frac{d}{x^2}\left(\frac{d}{x}-1\right)=0 \tag{38}$$

After simplification, it is

$$x=\frac{a^2+b^2c^2+d^2}{a+bc(b-1)+d} \tag{39}$$

Substituting equation (31) into equation (36) is

$$\begin{aligned}c&=2\left[\left(\frac{1}{E_1}+\frac{1}{E_2}\right)-\left(\frac{\nu_{12}}{E_1}+\frac{\nu_{21}}{E_2}\right)\right]\\d&=-\frac{2}{\nu_{t45}}\left(\frac{\nu_{13}}{E_1}+\frac{\nu_{23}}{E_2}\right)\end{aligned} \tag{40}$$

Thus

$$x=\frac{\frac{8}{E_{45}{}^2}+\frac{2}{\nu_{45}{}^2}\left[\left(\frac{1}{E_1}+\frac{1}{E_2}\right)-\left(\frac{\nu_{12}}{E_1}+\frac{\nu_{21}}{E_2}\right)\right]^2+\frac{2}{\nu^2{}_{t45}}\left(\frac{\nu_{13}}{E_1}+\frac{\nu_{23}}{E_2}\right)^2}{\frac{2}{E_{45}}+\frac{1}{\nu_{45}}\left(\frac{1}{\nu_{45}}-1\right)\left[\left(\frac{1}{E_1}+\frac{1}{E_2}\right)-\left(\frac{\nu_{12}}{E_1}+\frac{\nu_{21}}{E_2}\right)\right]-\frac{1}{\nu_{t45}}\left(\frac{\nu_{13}}{E_1}+\frac{\nu_{23}}{E_2}\right)} \tag{41}$$

$$S_{66}=\frac{1}{2}\left(x-S_{11}-S_{12}-S_{21}-S_{22}\right) \tag{42}$$

Substituting the correlation coefficient in equation (31) into equation (42) is

$$\begin{aligned}S_{66}=&\frac{\frac{4}{E_{45}{}^2}+\frac{1}{\nu_{45}{}^2}\left[\left(\frac{1}{E_1}+\frac{1}{E_2}\right)-\left(\frac{\nu_{12}}{E_1}+\frac{\nu_{21}}{E_2}\right)\right]^2+\frac{1}{\nu_{45}{}^2}\left(\frac{\nu_{13}}{E_1}+\frac{\nu_{23}}{E_2}\right)}{\frac{2}{E_{45}}+\frac{1}{\nu_{45}}\left(\frac{1}{\nu_{45}}-1\right)\left[\left(\frac{1}{E_1}+\frac{1}{E_2}\right)-\left(\frac{\nu_{12}}{E_1}+\frac{\nu_{21}}{E_2}\right)\right]-\frac{1}{\nu_{t45}}\left(\frac{\nu_{13}}{E_1}+\frac{\nu_{23}}{E_2}\right)}\\&-\frac{1}{2}\left(\frac{1}{E_1}+\frac{1}{E_2}\right)-\frac{1}{2}\left(\frac{\nu_{12}}{E_1}+\frac{\nu_{21}}{E_2}\right)\end{aligned} \tag{43}$$

In summary, when the metal sheet neither meets the necessary nor the sufficient conditions, the anisotropic coefficients S are obtained by numerically solving the unconstrained extremum stagnation point of the above error function. When the metal sheet does not meet the necessary conditions or sufficient conditions, the analytical expression of S_{66} is obtained by solving the extremum stagnation point of the endpoint constraint condition, and the shear modulus G_{12} is obtained.

It should be noted that in the case of metal sheets, the acquisition of the experimental value of Poisson's ratio in the thickness direction is severely limited by the accuracy of the measuring instrument. By analyzing the composition characteristics of equation (5), the anisotropic parameters related to Poisson's ratio in the thickness direction are S_{13} and S_{23}, and both only appear in the strain expression in the thickness direction. Therefore, when the practical application focuses on the calculation results of strain inside the sheet plane rather than the strain in the direction of sheet thickness, the third formula in equation (5) can be ignored. In this case, remove the relevant items of S_{13} and S_{23} in all the previous discussions. However, in this study, to calculate the error function more comprehensively, the Poisson's ratio in the thickness direction is taken as the experimental value at an angle of 45° with the rolling direction of the sheet.

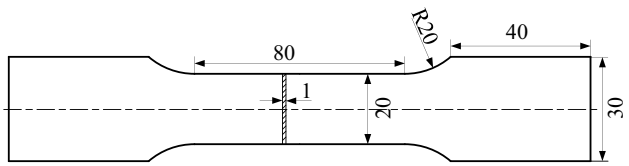

Fig. 2 Uniaxial tensile specimen size (mm)

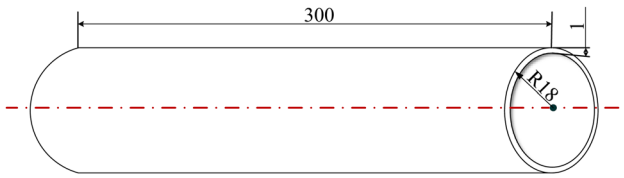

Fig. 3 Thin-walled tube torsion specimen size (mm)

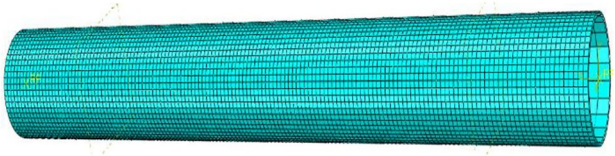

Fig. 4 Finite element model and meshing of thin-walled tube torsion test

Experiment

Uniaxial Tension Test

DC01, DC04, DC06 and 6061 sheets are selected as the research objects, the standard uniaxial tensile were sampled along the rolling direction of 0°, 15°, 30°, 45°, 60°, 75° and 90°, respectively. The size of the sample is shown in Fig. 2. The uniaxial tensile test was carried out on the Inspekt100kN electronic universal material testing machine, and the gauge elongation and width reduction during the tensile process were recorded by the longitudinal extensometer and the wide extensometer respectively. The average strain rate was 9E-4 s^{-1} for longitudinal strain at room temperature.

Thin-walled Tube Torsion Experiment

Different from the common uniaxial tensile experiment, the thin-walled tube torsion test has many difficulties, as mentioned above. Therefore, it is necessary to introduce the experiment in detail and carry out finite element simulation to verify the reliability of the experiment.

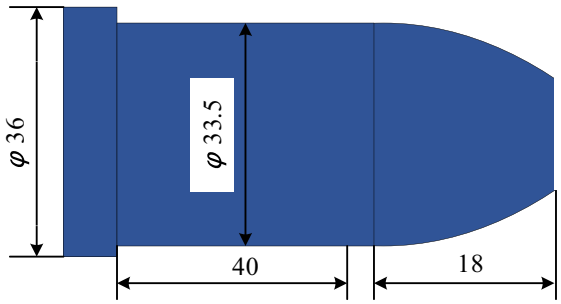

Fig. 6 Size of metal round plugs used to maintain tube end shape (mm)

Finite element model

The diameter of the thin-walled tube torsion specimen used should be as small as possible and the length as long as possible. But, considering the factors such as preparation conditions and test equipment, the designed specimen size is shown in Fig. 3.

The finite element model consists of a tube and two mandrels. The tube adopts the shell element type, and the mandrels adopt the discrete rigid body element type. The outer surface of the mandrels and the outer surface of both ends of the tube are set as coupling constraints. To ensure that the model is close to the actual torsion experiment, the boundary condition of the model is a fixed section, and the other end is applied with the torsion load. The model is meshed by hexahedral elements, as shown in Fig. 4.

Sample preparation and torsion experiment

The preparation process of the torsion sample is shown in Fig. 5.

Through the process shown in Fig. 5, the influence of the weld on the pipe sample can be minimized. To avoid the deformation of both ends of the circular tube due to the clamping force, a pair of metal plugs with the size shown in Fig. 6 was designed. The outer diameter of the plug and the inner diameter of the tube are clearance fit.

The torsion experiment was carried out on a 2ND3005 microcomputer-controlled electronic torsion testing

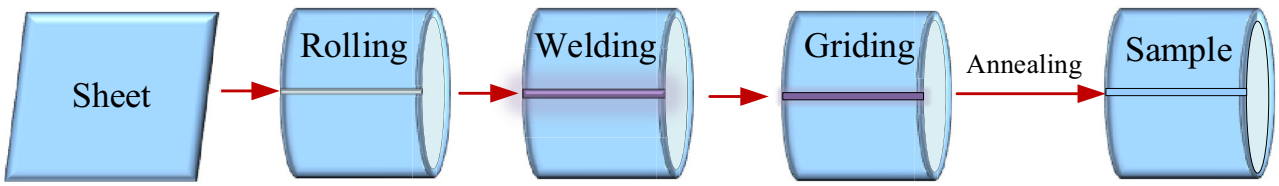

Fig. 5 Process diagram of torsion specimen to eliminate the influence of weld seam

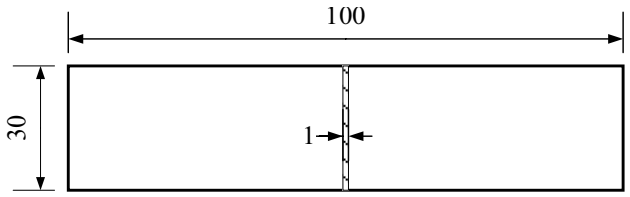

Fig. 7 V-bending specimen size (mm)

machine, and the deformation of the sample was recorded by sticking a strain gauge. The average torsion rate of the torsion specimen was 0.5°/min at room temperature.

V-bending Experiment

To verify the orthotropic elastic constitutive model, DC04 and 6061 were selected to carry out V- bending experiments in 0° and 90° directions.

Finite element model

The traditional isotropic elastic model and the established anisotropic elastic model were used to simulate the V-bending experiment. The finite element size and material property parameters of the specimen are shown in Fig. 7 and Table 1, respectively. In order to eliminate the influence factors other than anisotropic elasticity, the same hardening function is used for the bending deformation in different directions, which ensures that the bending deformation in different directions is affected by the equivalent plastic deformation.

As shown in Fig. 8, the finite element model consists of a punch, a die and a sample, where the die is a rotatable rigid body. The hexahedral element type is used to divide the mesh and the symmetry constraint is used to simplify the model. The punch fillet is 2 mm, the die fillet is 15 mm, and the die distance is 90 mm. When the model is working, the punch is pressed down 30 mm and then unloaded to obtain the sample after springback.

Table 1 Material property parameters

Material	Angle /°	E /MPa	N	Yield stress / MPa
DC04	0	191368	0.382	138
	90	212985	0.448	140
6061	0	72611	0.331	263
	90	72863	0.331	272

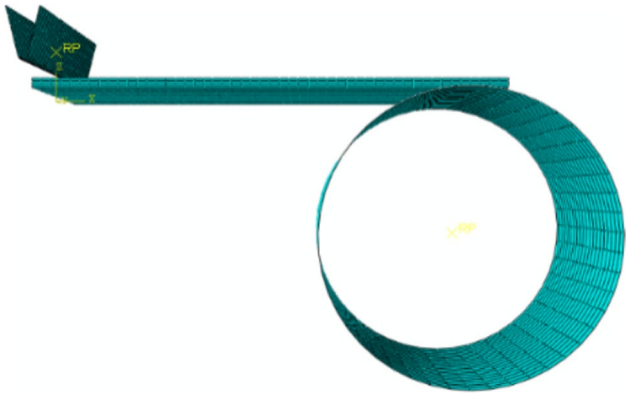

Fig. 8 One-half finite element model and meshing diagram of V-bending test

Experiment

The rectangular samples were cut at 0° and 90° along the rolling direction. The V-bending experiments were carried out on the mold shown in Fig. 9. The punch pressing rate was 5 mm/min at room temperature.

Results and Discussions

Uniaxial Tensile

The experimental curves of the elastic stage in seven directions are shown in Fig. 10, where S is true stress, HR is the strain in the longitudinal direction of the sample, TR is the strain in the transverse direction of the sample.

The elastic stage of the experimental curve is fitted to obtain the elastic constants. According to equations (7) and

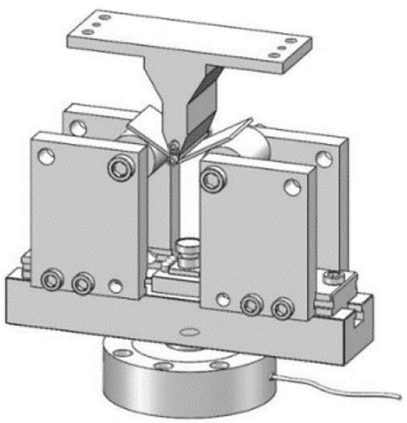

Fig. 9 3D die diagram of V-bending experimental equipment

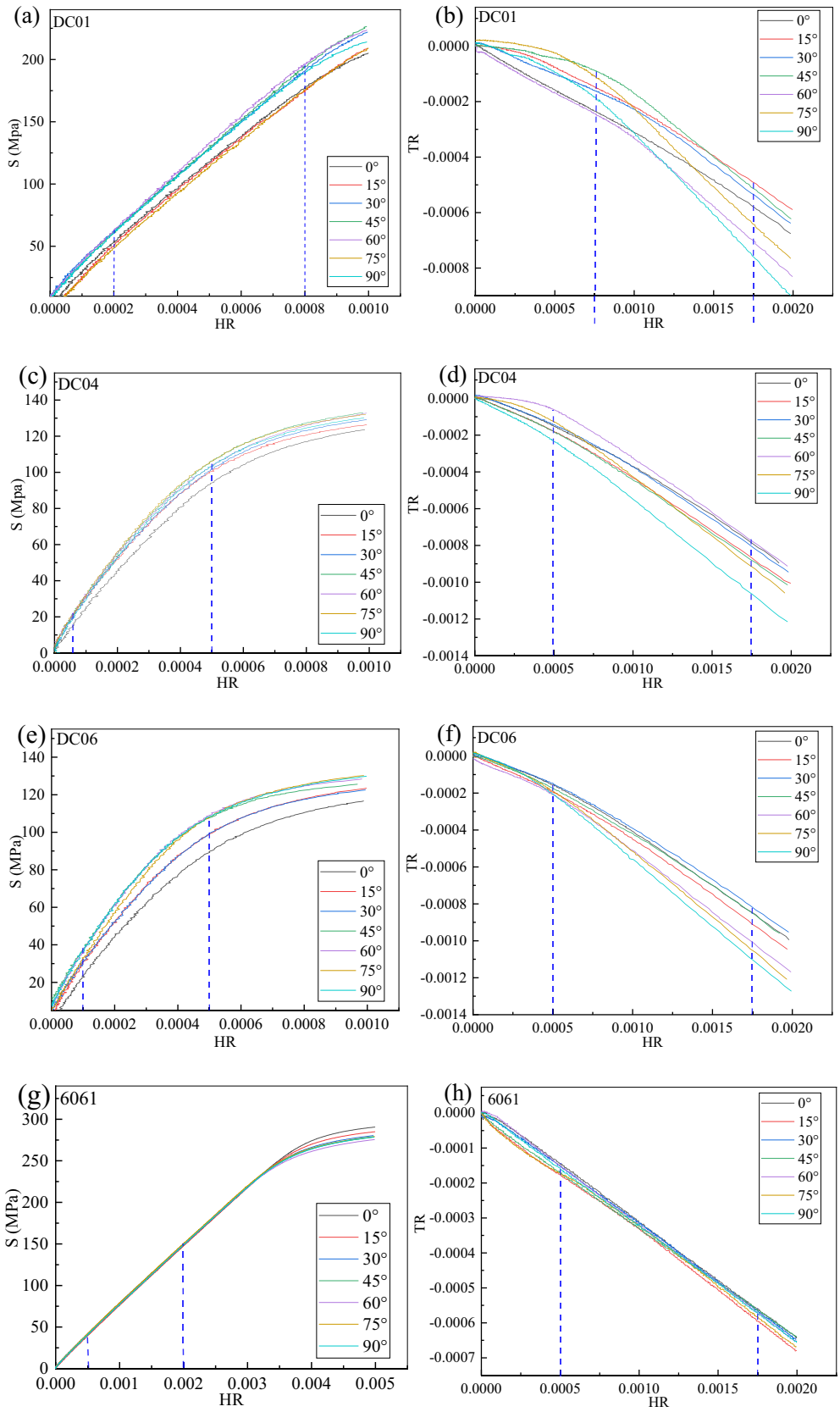

Fig. 10 Elastic stage curve of tensile test for the four materials, where the imaginary line is the value region of elastic parameters: Elastic modulus (**a**, **c**, **e**, **g**) Poisson's ratio (**b**, **d**, **f**, **h**)

Table 2 Calculation and judgment results of elastic constants

Material	Angle/°	E/MPa	ν	Necessary condition/%	Results	Sufficient condition/%	Results
DC01	0	206412	0.356	14.56	mismatch	4.02	match
	15	210575	0.304			2.05	
	30	218089	0.300			0.82	
	45	216750	0.276			4.65	
	60	220114	0.310			0.63	
	75	221231	0.309			0.28	
	90	211720	0.312			3.86	
DC04	0	191368	0.395	1.91	match	0.62	mismatch
	15	198374	0.423			6.79	
	30	198843	0.413			1.93	
	45	209505	0.422			4.27	
	60	206306	0.419			2.56	
	75	211013	0.414			4.69	
	90	212985	0.448			0.76	
DC06	0	191618	0.382	8.89	mismatch	2.75	mismatch
	15	200126	0.392			5.32	
	30	192759	0.378			5.46	
	45	205905	0.361			0.49	
	60	201874	0.363			4.22	
	75	207366	0.408			14.66	
	90	202059	0.367			1.10	
6061	0	72611	0.331	0.35	match	0.09	match
	15	73004	0.330			0.44	
	30	73155	0.329			0.41	
	45	73143	0.316			1.65	
	60	73179	0.337			1.39	
	75	73471	0.344			2.78	
	90	72863	0.331			0.09	

(22), calculate and judge whether the sheet meets the necessary and sufficient conditions. It should be noted that satisfying the necessary and sufficient conditions does not mean absolute equality. However, when the relative error between the two is less than 5%, the two are approximately equal. The calculation and judgment results are shown in Table 2.

Thin-walled Tube Torsion

The shear stress-strain curves and simulation results obtained from the torsion experiment are shown in Fig. 11. It can be seen from Fig. 11 that the simulation and test curves are close, indicating the reliability of the torsion test.

The experiment and simulation results of shear modulus shown in Table 3 were obtained by fitting the shear stress-strain elastic stage curve.

Error Function Calculation

For the convenience of expression, the above error function methods (ERFM) are renamed, and the new names are shown in Table 4.

According to the results of Table 2, DC01 only satisfies the sufficient condition, DC04 only satisfies the necessary condition, DC06 neither satisfies the sufficient condition nor the necessary condition, and 6061 satisfies both. Therefore, the DC06 is calculated using the ERFM1 and ERFM3 methods, and the DC01 and DC04 are calculated using the ERFM2 and ERFM4 methods. The solving results are given in Table 5.

The calculation results of ERFM1 and ERFM3 in Table 5 are brought into equations (14–16), and the elastic parameters in all directions are given in Table 6.

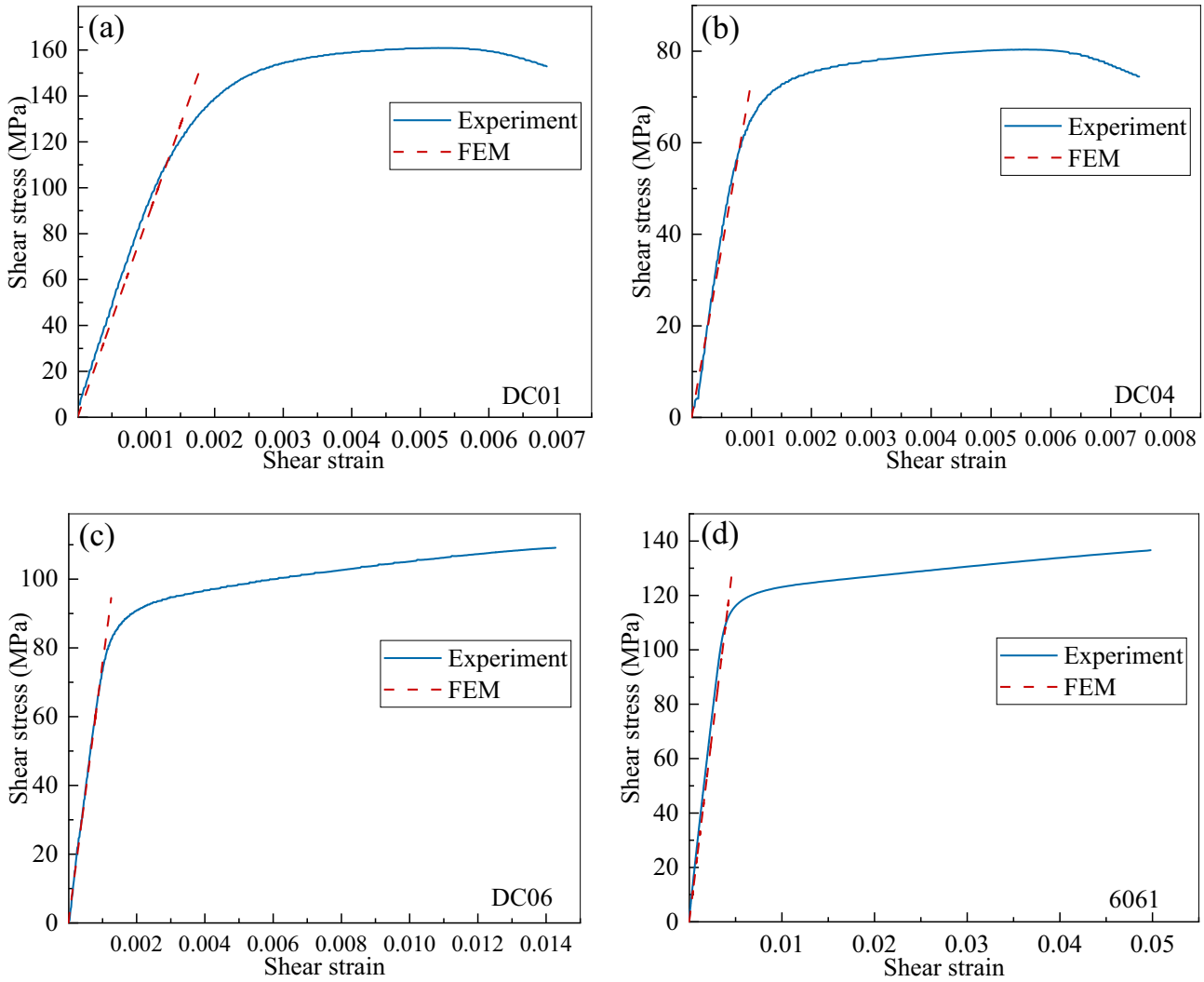

Fig.11 Experimental and simulated shear stress shear strain curves: (**a**) DC01, (**b**) DC04, (**c**) DC06, (**d**) 6061

Table 3 Experimental and simulated shear modulus

Material	DC01	DC04	DC06	6061
Experiment/MPa	87924	76642	77613	29057
FEM/MPa	84933	73666	75644	27798

Table 4 Renaming of ERFM

ERFM	Equation (29)	Equation (31)	Equation (33)	Equation (43)
New names	ERFM1	ERFM2	ERFM3	ERFM4

Figure 12 is the comparison results of the ERFM and the experiment. The comparison results show that the maximum relative error of elastic modulus is 3.62%, the maximum relative error of width-Poisson 's ratio is 8.82%, and the maximum relative error of thickness-Poisson 's ratio is 1.67%. It can be found from Fig. 12b that there are two abnormal convex points with large relative errors. If the experimental error is considered, such experimental points should be rounded off. Therefore, from the average value, the ERFM is proved to be reliable. In addition, compared with the ERFM1 overall, the average accuracy of the ERFM3 method is worse, but less than 5%. Therefore,

Table 5 Elastic coefficients calculated by ERFM

Methods	S_{11}	S_{12}	S_{13}	S_{22}	S_{23}	S_{66}
ERFM1	5.0632E-6	1.8886E-6	1.8144E-6	5.0280E-6	1.8019E-6	1.3440E-5
ERFM2						1.3279E-5
ERFM3	5.0233E-6	1.8623E-6	1.8168E-6	4.9835E-6	1.8024E-6	1.2789E-5
ERFM4						1.3293E-5

Table 6 Elastic modulus and Poisson's ratio calculated by ERFM1 and ERFM3

Angle/°		0	15	30	45	60	75	90
ERFM1	*E*/MPa	197504	198652	201059	202513	201773	199862	198886
	ν	-0.373	-0.37	-0.363	-0.361	-0.365	-0.372	-0.375
	ν_t	-0.362	-0.361	-0.630	-0.360	-0.360	-0.361	-0.362
ERFM3	*E*/MPa	199072	198,900	198634	198750	199422	200273	200662
	ν	-0.371	-0.364	-0.366	-0.365	-0.367	-0.372	-0.374
	ν_t	-0.358	-0.360	-0.364	-0.366	-0.364	-0.360	-0.358

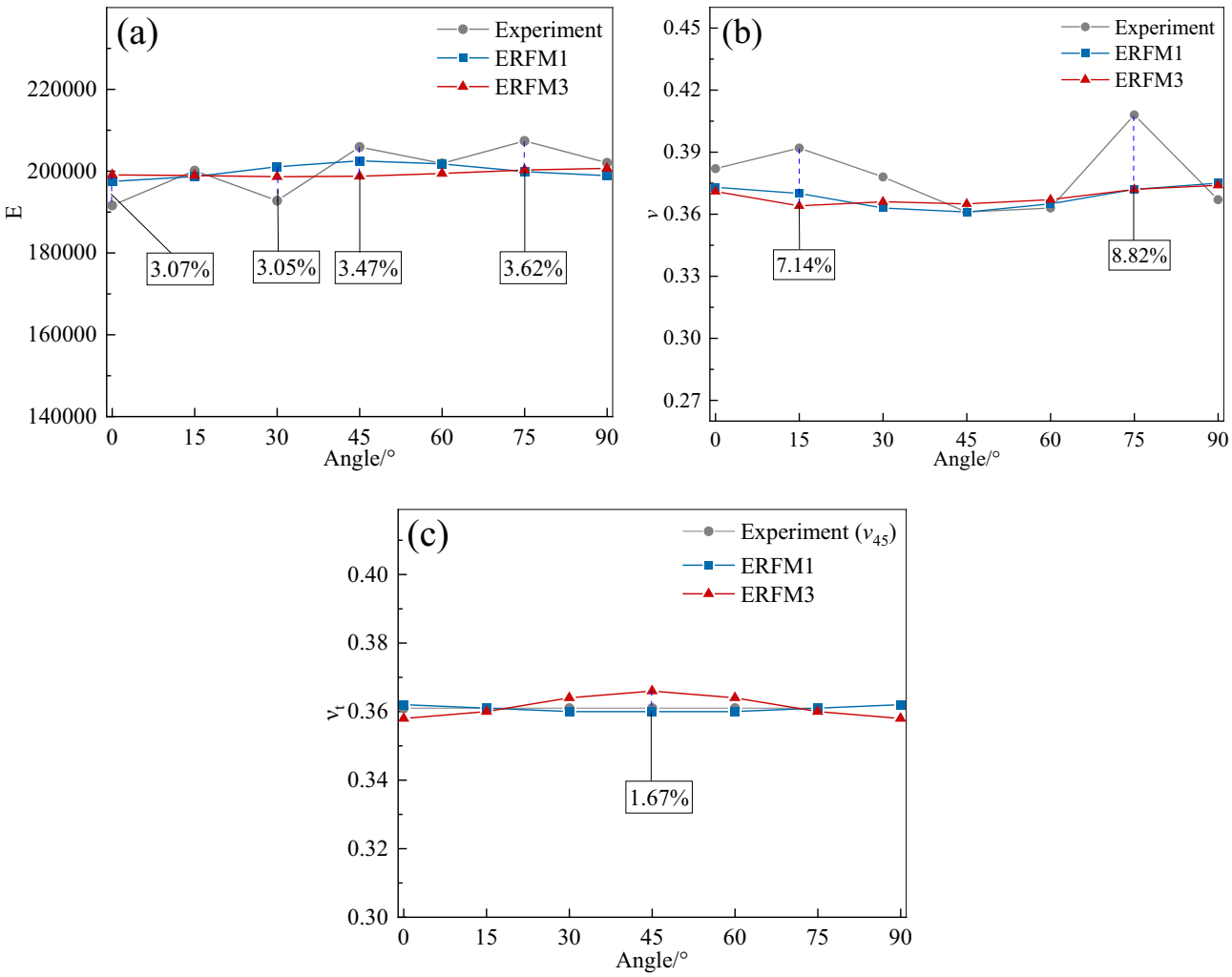

Fig. 12 Comparison of elastic parameters calculated by ERFM1,3 methods with experimental results: (**a**) E, (**b**) ν, (**c**) ν_t

Table 7 Shear modulus calculated by ERFM and equation (26) compare with experiment date

Methods	ERFM1	ERFM2	ERFM3	ERFM4	Equation (26)
G_{12}/MPa	74405	75309	75227	75228	27892
Relative error/%	4.13	1.74	3.07	1.84	4.00

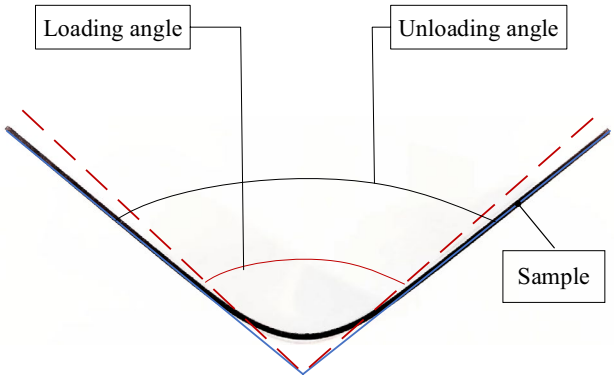

Fig. 13 Measurement method of springback angle after unloading

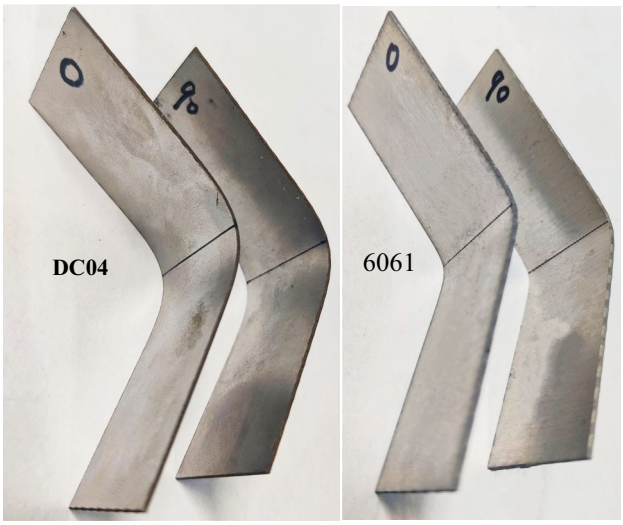

Fig. 14 The specimen after unloading

under the premise of satisfying the accuracy, the ERFM3 (the ERFM for three-group samples) can be selected to solve the parameters, which greatly reduces the experimental amount.

According to Table 5 and equation (26), the shear modulus G_{12} are given in Table 7. Figure 13 is the comparison of the Shear modulus between ERFM and the experiment. It can be seen from Fig. 13 that the maximum relative error between ERFM and the experiment is 4.13%, which proves the accuracy of the ERFM. In addition, for the orthotropic metal sheet, the shear modulus calculated by equation (26) is accurate.

V-bending Experiment

In the bending experiment, according to the principle of plastic work equivalence, the plastic strain of bending deformation in different directions is equal by calculating the downward pressure of bending, so the influence of plastic deformation in different directions is almost equivalent. The measurement of the springback angle of the specimen is shown in Fig. 13. The bending angle at loading is 94.4°. The specimens after unloading are shown in Fig. 14.

The comparison of V-bending experiments and simulation results of DC04 and 6061 is shown in Fig. 15. The columns in the figure are the simulation results of isotropic elastic model and anisotropic model, respectively. Where the dotted line is the bending angle of the specimen at loading, the red line is the bending angle of the specimen in the 0° direction after unloading, and the blue line is the bending angle of the specimen in the 90° direction after unloading.

In Fig. 15, the comparison between the red line and the blue line shows that there are obvious differences in the bending angles of the samples in different directions after unloading, which proves that anisotropic elasticity has an important influence on springback. However, this difference has not been well predicted by the isotropic elastic model, while the anisotropic elastic model shows satisfactory results, and the predicted springback differences in different directions are in good agreement with the experimental results.

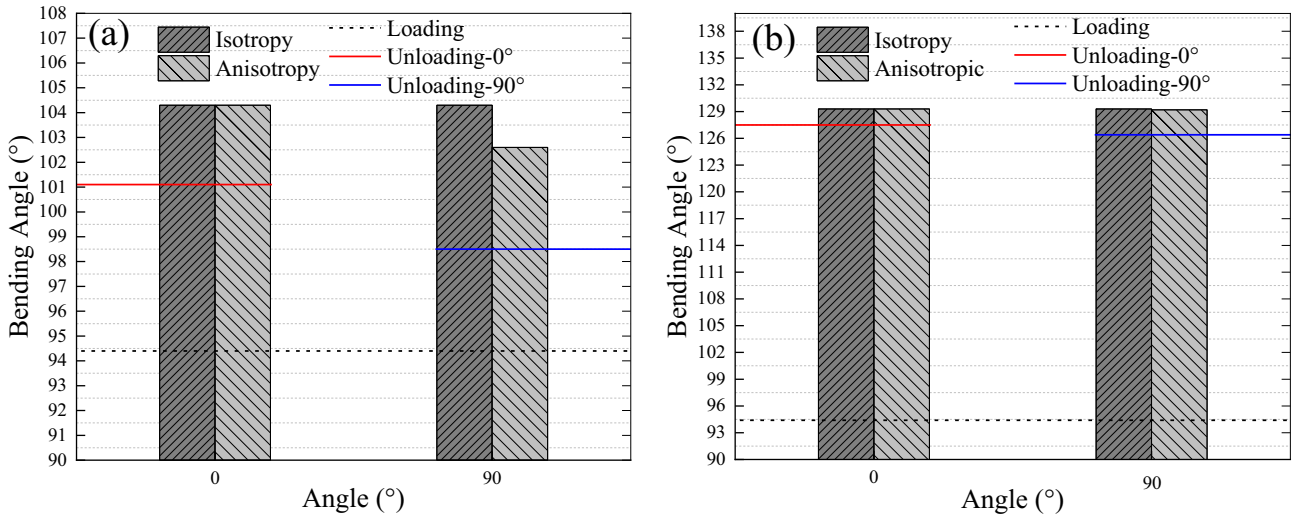

Fig.15 Comparison of V-bending experiment and simulation results: (**a**) DC04 (**b**) 6061

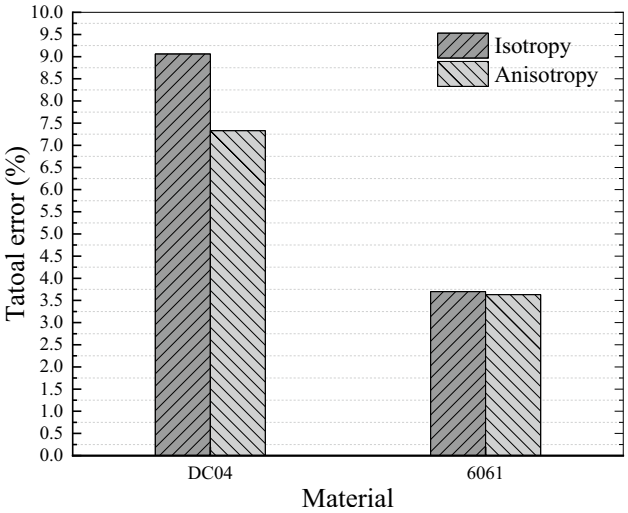

Fig.16 Comprehensive prediction errors of different elastic models

The comprehensive error function shown in equation (44) is established to evaluate the prediction accuracy of different elastic models. Equation (44) represents the sum of relative errors in different directions, that is, the comprehensive error. The calculation results of the error function are given in Fig. 16.

$$\zeta = \left(\left| \frac{{\theta_0}^{pre} - {\theta_0}^{exp}}{{\theta_0}^{exp}} \right| + \left| \frac{{\theta_{90}}^{pre} - {\theta_{90}}^{exp}}{{\theta_{90}}^{exp}} \right| \right) \times 100\% \qquad (44)$$

where ${\theta_\alpha}^{\mathrm{pre}}$ and ${\theta_\alpha}^{\mathrm{exp}}$ are the predicted and experimental values in the 0° and 90° directions, respectively.

It can be seen from Fig. 16 that the comprehensive error of the anisotropic elastic model is significantly smaller than that of the isotropic model, indicating that the anisotropic elastic model can significantly improve the prediction accuracy of springback. Combined with the necessary and sufficient conditions as well as Fig. 16, it can be concluded that 6061 satisfies both the necessary and sufficient conditions while DC04 only fulfills the necessary ones. Obviously, the comprehensive error of 6061 is smaller than that of DC04, indicating that the anisotropic elastic model has higher prediction accuracy for materials that meet the necessary and sufficient conditions.

Conclusion

Aiming at the problem of anisotropic springback in the forming process of sheet metals, an orthotropic elastic model was established that can effectively improve the problem, and the necessary and sufficient conditions for judging the applicability of the model were given. Considering the difficulty of calibrating model parameters, a precise and user-friendly numerical solution method has been proposed. The established orthotropic elastic model was verified through V-bending simulation and experimentation. The following conclusions are obtained:

1. The V-bending test results obtained from different orientations of the sheet exhibit significant variations, which proves the obvious influence of the anisotropic springback problem in the forming process of the rolled sheet metals.
2. Compared to the conventional isotropic elastic model, the established orthotropic elastic model can significantly enhance the accuracy of springback prediction.
3. A necessary and sufficient criterion for assessing the applicability of the model is proposed, which, when satisfied, enables the established orthotropic elastic model to more accurately predict springback.

4. The proposed error function extremum method for calibrating elastic parameters has good prediction accuracy, with an average relative error within 5%. The three-group sample solution method significantly reduces experimental and data processing workload, demonstrating the precision and user-friendliness of this method.

Prospect In this paper, the issue of anisotropic springback in sheet metals was investigated, but there are still numerous limitations that need to be addressed. Firstly, the linear elastic assumption of the elastic modulus fails to accurately describe the deformation-induced evolution of the elastic modulus in practical applications. Secondly, the proposed necessary and sufficient conditions only provide a rough assessment of satisfaction and non-satisfaction, lacking quantitative analysis of varying degrees of satisfaction as well as other related issues. The author shall delve deeper into these contents in the future.

Funding This project was funded and supported by National Natural Science Foundation of China (51975 509).

Data Availability The authors confirm that the data supporting the findings of this study are available within the article.

Declarations

Conflict of Interest The authors declare that they have no conflict of interest.

References

1. Hou H, Zhao G, Chen L, Li H (2021) Anisotropic springback models of FCC metal material under severe plastic compressive deformation. Int J Mech Sci 202–203:106513. https://doi.org/10.1016/j.ijmecsci.2021.106513
2. Merklein M, Allwood JM, Behrens B-A, Brosius A, Hagenah H, Kuzman K, Mori K, Tekkaya AE, Weckenmann A (2012) Bulk forming of sheet metal. CIRP Ann 61(2):725–745. https://doi.org/10.1016/j.cirp.2012.05.007
3. Marko V, Miroslav H, Bojan S, Boris S (2011) A new anisotropic elasto-plastic model with degradation of elastic modulus for accurate springback simulations. IntJ Mater Form 4(2):217–225. https://doi.org/10.1007/s12289-011-1029-8
4. Yoshida F, Amaishi T (2020) Model for description of nonlinear unloading-reloading stress-strain response with special reference to plastic-strain dependent chord modulus. Int J Plast 130:102708. https://doi.org/10.1016/j.ijplas.2020.102708
5. Sun L, Wagoner RH (2011) Complex unloading behavior: Nature of the deformation and its consistent constitutive representation. Int J Plast 27(7):1126–1144. https://doi.org/10.1016/j.ijplas.2010.12.003
6. Zajkani A, Hajbarati H (2017) Investigation of the variable elastic unloading modulus coupled with nonlinear kinematic hardening in springback measuring of advanced high-strength steel in U-shaped process. J Manuf Process 25:391–401. https://doi.org/10.1016/j.jmapro.2016.12.022
7. Zajkani A, Hajbarati H (2017) An analytical modeling for springback prediction during U-bending process of advanced high-strength steels based on anisotropic nonlinear kinematic hardening model. Int J Adv Manuf Technol 90(1–4):349–359. https://doi.org/10.1007/s00170-016-9387-5
8. Meng Q, Zhai R, Zhang Y, Fu P, Zhao J (2022) Analysis of springback for multiple bending considering nonlinear unloading-reloading behavior, stress inheritance and Bauschinger effect. J Mater Process Technol 307:117657. https://doi.org/10.1016/j.jmatprotec.2022.117657
9. Chang Y, Wang N, Wang BT, Li XD, Wang CY, Zhao KM, Dong H (2021) Prediction of bending springback of the medium-Mn steel considering elastic modulus attenuation. J Manuf Process 67(8):345–355. https://doi.org/10.1016/j.jmapro.2021.04.074
10. Aerens R, Vorkov V, Duflou JR (2019) Springback prediction and elasticity modulus variation. in: 18th International Conference on Sheet Metal (SHEMET) - New Trends and Developments in Sheet Metal Processing, KU, Dept Mech Engn, Leuven, Belgium. 185–192. https://doi.org/10.1016/j.promfg.2019.02.125
11. Liu X, Cao J, Chai X, Liu J, Zhao R, Kong N (2017) Investigation of forming parameters on springback for ultra high strength steel considering Young's modulus variation in cold roll forming. J Manuf Process 29:289–297. https://doi.org/10.1016/j.jmapro.2017.08.001
12. Yang X, Choi C, Sever NK, Altan T (2016) Prediction of springback in air-bending of Advanced High Strength steel (DP780) considering Young's modulus variation and with a piecewise hardening function. Int J Mech Sci 105:266–272. https://doi.org/10.1016/j.ijmecsci.2015.11.028
13. Mehrabi H, Yang CH, Wang BL (2021) Investigation on springback behaviours of hexagonal close-packed sheet metals. Appl Math Model 92(9):149–175. https://doi.org/10.1016/j.jmapro.2017.08.001
14. Lin J, Hou Y, Min J, Tang H, Carsley JE, Stoughton TB (2020) Effect of constitutive model on springback prediction of MP980 and AA6022-T4. IntJ Mater Form 13(9):1–13. https://doi.org/10.1016/j.ijmecsci.2019.05.046
15. Hajbarati H, Zajkani A (2019) A novel analytical model to predict springback of DP780 steel based on modified Yoshida-Uemori two-surface hardening model. IntJ Mater Form 12(3):441–455. https://doi.org/10.1007/s12289-018-1427-2
16. Ul Hassan H, Traphoener H, Guener A, Tekkaya AE (2016) Accurate springback prediction in deep drawing using pre-strain based multiple cyclic stress-strain curves in finite element simulation. Int J Mech Sci 110:229–241. https://doi.org/10.1016/j.ijmecsci.2016.03.014
17. Yoshida F (2022) Description of elastic-plastic stress-strain transition in cyclic plasticity and its effect on springback prediction. IntJ Mater Form 15(2):12. https://doi.org/10.1007/s12289-022-01651-1
18. Seo KY, Kim JH, Lee HS, Kim JH, Kim BM (2018) Effect of Constitutive Equations on Springback Prediction Accuracy in the TRIP1180 Cold Stamping. Metals 8(1):18. https://doi.org/10.3390/met8010018
19. Meng Q, Zhao J, Mu Z, Zhai R, Yu G (2022) Springback prediction of multiple reciprocating bending based on different hardening models. J Manuf Process 76:251–263. https://doi.org/10.1016/j.jmapro.2022.01.070
20. Li Y, Liang Z, Zhang Z, Zou T, Li D, Ding S, Xiao H, Shi L (2019) An analytical model for rapid prediction and compensation of springback for chain-die forming of an AHSS U-channel. Int J Mech Sci 159:195–212. https://doi.org/10.1016/j.ijmecsci.2019.05.046
21. Xue X, Liao J, Vincze G, Sousa J, Barlat F, Gracio J (2016) Modelling and sensitivity analysis of twist springback in deep drawing

of dual-phase steel. Mater Des 90:204–217. https://doi.org/10.1016/j.matdes.2015.10.127
22. Hajbarati H, Zajkani A (2020) A novel finite element simulation of hot stamping process of DP780 steel based on the Chaboche thermomechanically hardening model. Int J Adv Manuf Technol 111:2705–2718. https://doi.org/10.1007/s00170-020-06297-4
23. Choi Y, Lee J, Panicker SS, Jin HK, Panda SK, Lee MG (2020) Mechanical properties, springback, and formability of W-temper and peak aged 7075 aluminum alloy sheets: Experiments and modeling. Int J Mech Sci 170:105344. https://doi.org/10.1016/j.ijmecsci.2019.105344
24. Julsri W, Suranuntchai S, Uthaisangsuk V (2018) Study of springback effect of AHS steels using a microstructure based modeling. Int J Mech Sci 135:499–516. https://doi.org/10.9773/sosei.55.949
25. Sumikawa S, Ishiwatari A, Hiramoto J (2017) Improvement of springback prediction accuracy by considering nonlinear elastoplastic behavior after stress reversal. J Mater Process Technol 241:46–53. https://doi.org/10.1016/j.jmatprotec.2016.11.005
26. Sumikawa S, Ishiwatari A, Hiramoto J, Urabe T (2016) Improvement of springback prediction accuracy using material model considering elastoplastic anisotropy and Bauschinger effect. J Mater Process Technol 230:1–7. https://doi.org/10.1016/j.jmatprotec.2015.11.004
27. Leu DK (2019) Relationship between mechanical properties and geometric parameters to limitation condition of springback based on springback-radius concept in V-die bending process. Int J Adv Manuf Technol 101:913–926. https://doi.org/10.1007/s00170-018-2970-1
28. Zhu YX, Chen W, Li HP, Liu YL, Chen L (2018) Springback study of RDB of rectangular H96 tube. Int J Mech Sci 138:282–294. https://doi.org/10.1016/j.ijmecsci.2018.02.022
29. Ouakdi EH, Louahdi R, Khirani D, Tabourot L (2012) Evaluation of springback under the effect of holding force and die radius in a stretch bending test. Mater Des 35:106–112. https://doi.org/10.1016/j.matdes.2011.09.003
30. Zhai R, Ding X, Yu S, Wang C (2018) Stretch bending and springback of profile in the loading method of prebending and tension. Int J Mech Sci 144:746–764. https://doi.org/10.1016/j.ijmecsci.2018.06.028
31. Wang A, Xue H, Saud S, Yang Y, Wei Y (2019) Improvement of springback prediction accuracy for Z-section profiles in four-roll bending process considering neutral layer shift. J Manuf Process 48:218–227. https://doi.org/10.1016/j.jmapro.2019.11.008
32. Kut S, Stachowicz F, Pasowicz G (2021) Springback Prediction for Pure Moment Bending of Aluminum Alloy Square Tube. Materials 14(14):3814. https://doi.org/10.3390/ma14143814
33. Zhan M, Xing L, Gao PF, Ma F (2019) An analytical springback model for bending of welded tube considering the weld characteristics. Int J Mech Sci 150:594–609. https://doi.org/10.1016/j.ijmecsci.2018.10.060
34. Ailinei L, Galatanu SV, Marsavina L (2012) Influence of anisotropy on the cold bending of S600MC sheet metal. Eng Fail Anal 137:106206. https://doi.org/10.1016/j.engfailanal.2022.106206
35. Aleksandrović S, Ivković D, Arsic D, Делић M, Djačić S, Djordjevic MT (2023) Effect of plastic strain and specimen geometry on plastic strain ratio values for various materials. Adv Technol Mater 28(1):13–19. https://doi.org/10.24867/ATM-2023-1-003
36. Wu F, Hong Y, Zhang Z, Huang C, Huang Z (2023) Effect of Lankford Coefficients on Springback Behavior during Deep Drawing of Stainless Steel Cylinders. Materials 16(12):4321. https://doi.org/10.3390/ma16124321
37. Kut S, Pasowicz G, Stachowicz F (2023) On the Springback and Load in Three-Point Air Bending of the AW-2024 Aluminium Alloy Sheet with AW-1050A Aluminium Cladding. Materials 16(8):2945. https://doi.org/10.3390/ma16082945
38. Miksza M, Bohdal L, Kaldunski P, Patyk R, Leon K (2022) Forecasting the Fatigue Strength of DC01 Cold-Formed Angles Using the Anisotropic Barlat Model. Materials 15(23):8436. https://doi.org/10.3390/ma15238436
39. Aretz H (2005) A non-quadratic plane stress yield function for orthotropic sheet metals. J Mater Process Technol 168(1):1–9. https://doi.org/10.1016/j.jmatprotec.2004.10.008
40. Tong W, Alharbi M, Sheng J (2020) On the new shear constraint for plane-stress orthotropic plasticity modeling of sheet metals. Exp Mech 60(7):889–905. https://doi.org/10.1007/s11340-020-00596-3
41. Yin Q, Soyarslan C, Güner A, Brosius A, Tekkaya AE (2012) A cyclic twin bridge shear test for the identification of kinematic hardening parameters. Int J Mech Sci 59(1):31–43. https://doi.org/10.1016/j.ijmecsci.2012.02.008
42. Ballo F, Gobbi M, Mastinu G, Previati G (2020) Thin-walled tubes under torsion: multi-objective optimal design. Optim Eng 21:1–24. https://doi.org/10.1007/s11081-019-09431-8
43. Bhaduri A (2018) Torsion—Pure Shear. In: Mechanical Properties and Working of Metals and Alloys. Springer Singapore. 264:197–225. https://doi.org/10.1007/978-981-10-7209-3_5
44. Bailey JA, Haas SL, Nawab KC (1972) Anisotropy in Plastic Torsion. J Basic Eng 94:231–237. https://doi.org/10.1115/1.3425374
45. White CS (1992) An Analysis of the Thin-Walled Torsion Specimen. J Eng Mater Technol 114:384–389. https://doi.org/10.1115/1.2904189
46. Peng X, Qin Y, Balendra R (2001) Finite element investigation into the torsion test in the range of large strains and deformations. J Strain Anal Eng Des 36:401–409. https://doi.org/10.1243/0309324011514566
47. Ramagiri B, Yerramalli CS (2021) Numerical investigation on the effect of specimen gripping arrangement on dynamic shear characterization using Torsion Split Hopkinson Bar. Eur Phys J Web Conf 250(4):02032. https://doi.org/10.1051/epjconf/202125002032